

CSI-free vs CSI-based multi-antenna WET schemes for massive low-power Internet of Things

Onel L. A. López, Nurul Huda Mahmood, Hirley Alves, Matti Latva-aho

Abstract—Wireless Energy Transfer (WET) is emerging as a promising solution for powering massive Internet of Things (IoT) deployments. An important question that has recently raised the interests from the research community is whether the costly Channel State Information (CSI) acquisition procedure is necessary for optimum performance. In this paper, we shed some light into this matter by evaluating CSI-based and CSI-free multi-antenna WET schemes in a Wireless Powered Communication Network (WPCN) with WET in the downlink, and periodic or Poisson-traffic Wireless Information Transfer (WIT) in the uplink. When CSI is available, we show that a Maximum Ratio Transmission beamformer is close to optimum whenever the farthest node experiences at least 3 dB of power attenuation more than the remaining devices. On the other hand, although the adopted CSI-free mechanism is not capable of providing average harvesting gains, it does provide greater WET/WIT diversity gains with lower energy requirements when compared with the CSI-based scheme. Our numerical results evidence that the CSI-free scheme constitutes the optimum for most of the configurations; although its performance may degrade significantly if the setup is not optimally configured in case of Poisson traffic. Finally, we show the prominent performance results when the uplink transmissions are periodic, while highlighting the need of using a minimum mean square error equalizer rather than zero-forcing for information decoding.

Index Terms—WET, massive IoT, WPCN, CSI-free, energy beamforming, periodic traffic, Poisson traffic, MMSE, ZF

I. INTRODUCTION

The Internet of Things (IoT) is a major technology trend that promises to interconnect *everything* towards building a data-driven society enabled by near-instant unlimited wireless connectivity [1], [2]. A key feature/challenge of the IoT is the massive connectivity since around 80 billion connected devices are foreseen to proliferate globally by 2025, thus resulting in a massive technology-led disruption across all industries [3].

The IoT ranges from cloud (e.g., data centers, super computers, internet core network) and fog (e.g., computers, smart-phones, smart appliances) technologies, to edge (e.g., wearables, smart sensors, motes) and extreme edge (e.g., smart dust and zero-power sensors) technologies [4]. Energy efficiency and/or power consumption criteria become more critical as one descends over such layers. In fact, edge or extreme edge devices are usually powered by batteries or energy harvesters and are very limited in computing and storage capabilities to reduce costs and enlarge lifetime. Many types of energy

harvesting (EH) technologies are under consideration, e.g., based on solar, piezoelectric energy sources; but those relying on wireless radio frequency (RF) signals are becoming more and more attractive. RF-EH provides key benefits such as [5], [6]: i) battery charging without physical connections, which significantly simplify the servicing and maintenance of battery-powered devices; ii) readily available service in the form of transmitted energy (TV/radio broadcasters, mobile base stations and handheld radios), iii) low cost and form factor reduction of the end devices; iv) increase of durability and reliability of end devices thanks to their contact-free design; and v) enhanced energy efficiency and network-wide reduction of emissions footprint.

RF-EH is a wide concept¹ that encompasses two main scenarios when combined with Wireless Information Transfer (WIT), namely Wireless Powered Communication Network (WPCN) and Simultaneous Wireless Information and Power Transfer (SWIPT) [6]. In the first scenario, a Wireless Energy Transfer (WET) process occurs in the downlink in a first phase and WIT takes place in the second phase. Meanwhile, in the second scenario, WET and WIT occur simultaneously. An overview of the recent advances on both architectures can be found in [8], while herein the discussions will focus on WPCN and pure WET setups. Notice that WET may have a much more significant role than WIT in practical applications as highlighted in [6]. This is because WET's duration is often required to be the largest i) in order to harvest usable amounts of energy, and/or ii) due to sporadic WIT rounds, e.g., event-driven traffic. Since SWIPT may happen just occasionally, WPCN use cases are often of much more practical interest. Therefore, enabling efficient WPCNs is mandatory [2], [6], [9], and constitutes the scope of this work.

A. Related Work

Over the past few years, the analysis and optimization of WPCNs has evolved from the simple Harvest-then-Transmit (HTT) protocol [10]–[12] towards more evolved alternatives that are capable of boosting the system performance either via cooperation [13], power control [14], rate allocation schemes [15] and/or retransmissions [16]. However, most of the works so far are concerned with rather optimistic setups where either i) most of the power consumption sources at the EH devices are ignored, ii) Channel State Information (CSI) procedures

Authors are affiliated to the Centre for Wireless Communications (CWC), University of Oulu, Finland. {onel.alcarazlopez,nurullhuda.mahmood,hirley.alves,matti.latva-aho}@oulu.fi

This work is supported by Academy of Finland (Aka) (Grants n.307492, n.318927 (6Genesis Flagship), n.319008 (EE-IoT)).

¹Herein we focus on RF-EH networks where the RF signals are intentionally transmitted for powering the EH devices. Alternatively, the devices may opportunistically harvest energy from RF signals of different frequencies already in their surrounding environment and to which they are sensitive. The latter is known as ambient RF EH, and readers can refer to [7] for an overview.

are assumed cost free, and iii) only one or few EH devices are powered. Regarding the latter, the number of EH devices is often not greater than the number of powering antennas such that full gain from energy beamforming (EB) is attained in the WET phase, e.g., [12], [17], [18]. For instance, a setup where a multi-antenna hybrid access point (HAP) transfers power to the devices via EB, followed by the devices sending their data simultaneously by consuming the harvested energy, is investigated in [17]. The authors cast a max-min rate optimization problem with practical non-linear EH and solve it via several iterative optimization methods. However, no other power consumption sources besides transmissions are considered, and Zero Forcing (ZF) equalization is used for information decoding at the HAP without analysing the CSI acquisition costs. Meanwhile, the authors in [18] do consider the CSI acquisition costs when optimizing the HAP pilots power and the power allocated to the energy transmission, while the EH devices are under the effect of several power consumption sources. Yet, the imposition of having more antennas than devices may be strong towards future low-power massive IoT networks. Finally, the lack of a traffic source model for data transmissions is also a strong limitation for most of the works, which intrinsically assume full-buffer EH devices, e.g., [10]–[18].

One important observation is that the gains from EB decrease quickly as the number of EH IoT devices increases [6]. This holds even without accounting for the considerable energy resources demanded by CSI acquisition. Therefore, in massive deployment scenarios, the broadcast nature of wireless transmissions should be intelligently exploited for powering simultaneously a massive number of IoT devices with minimum or no CSI. To that end, the authors in [19] propose a new form of signal design for WET relying on phase sweeping transmit diversity, which forces the multiple antennas to induce fast fluctuations of the wireless channel and does not rely on any form of CSI. This is accomplished by exploiting the non-linearity of the EH circuitry. Meanwhile, several multi-antenna CSI-free WET solutions have been recently proposed and analyzed in [20], [21] to improve the statistics of the RF energy availability at the input of the EH circuitry of a massive set of energy harvesters:

- One Antenna (OA), under which the power beacon (PB) uses only one antenna transmitting with full power;
- All Antennas transmitting the Same Signal (AA – SS), under which the PB transmits the same signal simultaneously with all antennas but with equal, hence proportionally reduced, power at each;
- All Antennas transmitting Independent Signals (AA – IS), under which the PB transmits power signals independently generated across the antennas; and
- Switching Antenna (SA), under which the PB transmits with full power by one antenna at a time such that all antennas are used during a coherence block.

Notice that i) OA is the simplest scheme since it does not take advantage of the multiple spatial resources, while ii) AA – SS may reach considerable gains in terms of average harvested energy under Line of Sight (LOS) but it is highly

sensitive to the different mean phases of the LOS channel component, and iii) AA – IS, SA do not improve the average energy availability but do provide transmit diversity. It was demonstrated in [21] that devices closer to the PB benefit more from AA – IS, while those that are far, and more likely to operate near their sensitivity level, benefit more from the SA. All these CSI-free WET schemes have been considered without the information communication component typical of a WPCN, and consequently, their influence on the overall system performance is so far unclear.

B. Contributions and Organization of the Paper

This paper aims at analyzing for the first time the gains from operating with/without CSI for powering massive low-power IoT deployments with uplink transmission requirements. Specifically, we consider a WPCN where a massive set of IoT nodes require occasional uplink information transmissions to a HAP, which in turn is constantly transferring RF energy to them in the downlink. Herein, we adopt the SA strategy [20], [21] as the CSI-free WET scheme, which, besides the benefits aforementioned, allows a better coupling to the co-located information transmission processes. The latter is because only one antenna is used for WET at any time, while the remaining antennas stay silent, thus such idle antennas may be used for uplink information decoding in WPCN setups. The main contributions of this work are listed as follows:

- We investigate and analyze a WPCN setup under CSI-based and CSI-free powering schemes. We are concerned with the overall outage probability, which encompasses both WET and WIT processes' failures. The performance is evaluated in terms of the worst node's performance such that we can assure Quality of Service (QoS) guarantees for all nodes in the network. We consider the power consumption from several sources, e.g., transmission, circuitry, and CSI-acquisition procedures;
- We decouple WET and WIT processes and cast a max-min WET optimization problem when CSI is available at the HAP. We provide analytical bounds on the performance of the CSI-based WET beamforming by relying on Maximum Ratio Transmission (MRT). We show that the MRT is near the fairest EB, e.g., the EB that provides max-min performance guarantees, even in a massive deployment, if the farthest EH node experiences at least 3 dB of power attenuation more than the remaining devices;
- We consider two types of information traffic sources: i) periodic traffic, such that the network is perfectly synchronized; and ii) Poisson traffic, which is uncoordinated and random. The overall performance is analyzed for both traffic profiles. Our results not only evidence that the system performance deteriorates under Poisson random access when compared to deterministic traffic, but also that it is more challenging to optimally configure the network. We cast an optimization problem to determine the optimum pilot reuse factor such that the collision probability keeps below a certain limit. A solution algorithm is provided and shown to converge in few iterations;

- For information decoding in the uplink, the HAP implements either ZF or the Minimum Mean Square Error (MMSE) equalization. We show that the MMSE provides large performance gains for the WPCN under consideration when compared to ZF, mainly because of the low-rate low-power transmissions, which are typical in the analyzed scenario;
- The impact of the CSI-based and CSI-free scheme on the WET performance is analytically analyzed and several trade-offs are identified. It is shown that the CSI-free scheme is preferable as the number of IoT devices increases and/or the CSI acquisition costs increase. In terms of overall performance, the CSI-free scheme is shown to be the optimum for most of the configurations; although its performance may degrade significantly if the setup is not optimally configured in case of Poisson traffic.

Next, Section II presents the system model and assumptions, Section III discusses the energy outage performance under the CSI-based and CSI-free WET schemes, while Section IV addresses the information outage performance under ZF and MMSE decoding schemes. Section V presents and discusses numerical results. Finally, Section VI concludes the paper.

Notation: Boldface lowercase letters denote column vectors, while boldface uppercase letters denote matrices. For instance, $\mathbf{x} = \{x_i\}$ where x_i is the i -th element of vector \mathbf{x} ; while $\mathbf{X} = \{X_{i,j}\}$ where $X_{i,j}$ is the i -th row j -th column element of matrix \mathbf{X} . By \mathbf{I} we denote the identity matrix, and by $\mathbf{1}$ we denote a vector of ones. Superscripts $(\cdot)^T$ and $(\cdot)^H$ denote the transpose and conjugate transpose operations, while $\text{Tr}(\cdot)$ and $\text{diag}(\mathbf{x})$ denote the trace operator and a diagonal matrix with elements $\{x_i\}$, respectively. \mathbb{C} , \mathbb{R} and \mathbb{Z}^+ are the set of complex, real and non-negative integer numbers, respectively; while $i = \sqrt{-1}$ is the imaginary unit and $\Im(x)$ denotes the imaginary part of $x \in \mathbb{C}$. The absolute/cardinality operations in case of scalars/sets is denoted as $|\cdot|$, while $\|\mathbf{x}\|$ denotes the euclidean norm of vector \mathbf{x} . Additionally, $\lfloor \cdot \rfloor$ and $\lceil \cdot \rceil$ are the floor and ceiling functions, respectively, while $\sup\{\cdot\}$ and $\inf\{\cdot\}$ are the supremum and infimum notations. The curled inequality symbol \succeq is used to indicate positive definiteness of a matrix, while $\mathcal{O}(\cdot)$ is the big-O notation. $\mathbb{E}_X[\cdot]$ denotes expectation with respect to random variable (RV) X , which is characterized by a Probability Density Function (PDF) $f_X(x)$ and Cumulative Distribution Function (CDF) $F_X(x)$, while $\mathbb{P}[A]$ is the probability of event A . Also, $\sum_Y X$ denotes the sum of Y RVs distributed as $f_X(x)$. $\mathbf{c} \sim \mathcal{CN}(\boldsymbol{\mu}, \mathbf{R})$ is a circularly-symmetric Gaussian complex random vector, with mean vector $\boldsymbol{\mu}$ and covariance matrix \mathbf{R} , while $Y \sim \chi^2(\varphi, \psi)$ is a non-central chi-squared RV with φ degrees of freedom and parameter ψ such that [22]

$$F_Y(y) = 1 - \mathcal{Q}_{\varphi/2}(\sqrt{\psi}, \sqrt{y}), \quad (1)$$

where $\mathcal{Q}_a(\cdot)$ denotes the Marcum Q-function.

II. SYSTEM MODEL

We consider the scenario depicted in Fig. 1. In the downlink, a HAP wirelessly powers a large set $\mathcal{S} = \{s_i\}$ of S single-antenna EH sensor nodes located nearby. Such low-power

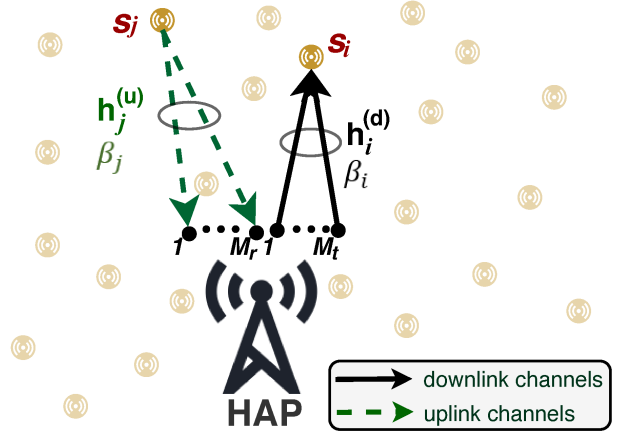


Fig. 1. System model: a HAP equipped with M antennas powers wirelessly in the downlink a set \mathcal{S} of single-antenna sensor nodes located nearby, while it receives information from a subset of them in the uplink.

devices require in turn to sporadically send some short data messages of k bits/Hz over time blocks of t seconds in the uplink. The HAP is equipped with M antennas, M_t of which are used for downlink energy transmission, and the remaining $M_r = M - M_t$ for information decoding in the uplink. We assume that the coherence time T_c is sufficiently large such that $t \leq T_c/M$ for any feasible M . On the one hand, notice that since the RF-EH devices are extremely-low-power nodes, they are foreseen to be mostly static devices, thus, the coherence time is large. On the other hand, such devices are expected to transmit for short times due to intrinsically small data payloads, low-latency requirements, and/or lack of energy resources to support longer transmissions [23]. Then, by limiting for instance the analysis of this work to $M \leq M_0$ we can set $t = T_c/M_0$, although extending any of our analyses for any other smaller t would be straightforward.

A. Channel model

The average channel gain between the HAP and s_i is denoted as β_i , e.g. the path loss is $1/\beta_i$, while the small-scale fading channel coefficient between the HAP's antennas and s_i (downlink) is denoted as $\mathbf{h}_i^{(d)} \in \mathbb{C}^{M_t \times 1}$, and the channel between s_i and HAP's antennas (uplink) is denoted as $\mathbf{h}_i^{(u)} \in \mathbb{C}^{M_r \times 1}$. Notice that even when the network is configured to operate over the same frequency band in uplink and downlink, the channel reciprocity is difficult to hold in this kind of setup since devices at both ends are extremely different [24], hence we assume fully independent uplink and downlink channels².

The antenna elements are sufficiently separated such that the fading seen at each antenna can be assumed independent. We assume quasi-static channels undergoing Rician fading, i.e., $\mathbf{h}_i^{(d)}, \mathbf{h}_i^{(u)} \sim \mathcal{CN}(\sqrt{\frac{\kappa}{1+\kappa}} \mathbf{1}_{M_{\{t,r\}} \times 1}, \frac{1}{1+\kappa} \mathbf{I}_{M_{\{t,r\}} \times M_{\{t,r\}}})$, which is a very general assumption that allows modeling a

²Even when certain dependence may exist, this does not affect significantly our results. This is because WIT phases in WPCNs are mostly sporadic, then, the aggregated harvested energy between consecutive WIT phases is much less dependent on the fading experienced in a particular coherence block.

wide variety of channels by tuning the Rician factor $\kappa \geq 0$ [25, Ch.2], e.g., when $\kappa = 0$ the channel envelope is Rayleigh distributed, while when $\kappa \rightarrow \infty$ there is a fully deterministic LOS channel.

B. Transmission model

We assume homogeneous (in terms of hardware, supported services and traffic characterization) IoT devices which are harvesting RF energy from HAP's transmissions. They require p_c power units to keep active, otherwise they are in outage. Such a value obviously depends on their circuitry but also on the services they require to support. Additionally, the EH devices need to report their data to the HAP at some moments, so they interrupt briefly (during t seconds) their EH process to send it. We model such transmission activation in two different ways, by considering:

- periodic traffic, such that the network is perfectly synchronized and every EH device has a predefined slot allocated for transmission. If the periodicity is t_s , then there are $\lfloor t_s/t \rfloor$ slots available. If $S \leq \lfloor t_s/t \rfloor$, then each device operates alone in the channel; otherwise there will be up to $\lceil S/\lfloor t_s/t \rfloor \rceil$ concurrent transmissions eventually;
- Poisson traffic, such that the network traffic is uncoordinated. Let us take λ as the mean number of messages per coherence time that are required to be transmitted by each EH device. Notice that it is evident that $\lambda < 1$ needs to hold according to our previous discussions.

It is worth noting that neither the periodic nor the Poisson model are suitable for mimicking bursty traffic, for which other more suitable models are recommended, e.g., [26]. However, a WPCN implementation is not suitable in scenarios requiring bursty transmissions mostly due to its inherent and strict energy limitations, thus we resorted to the above simple but effective models covering two extreme ends. Additionally, note that the multiple antennas at the HAP require to be exploited for spatially separating the concurrent transmissions with high reliability. We delve into the specific details in Section IV.

Finally, p_i denotes the fixed transmit power of s_i , while $\xi_{\text{csi}}^{(u)}$, $\xi_{\text{csi}}^{(d)}$ represent the energy resources³ (power \times time) utilized by such EH node to let the HAP know the uplink and downlink CSI, respectively. Notice that since channel reciprocity does not hold, it is expected that $\xi_{\text{csi}}^{(u)} < \xi_{\text{csi}}^{(d)}$ as transmissions from the EH devices are required in both downlink and uplink (pilot transmissions in uplink, feedback in downlink), but decoding/processing the pilots sent by the HAP is also required in the downlink.

C. Performance evaluation

We adopt the outage probability formulation as the main performance metric. We say s_i is in outage when: i) the harvested energy was insufficient for supporting its operation and consequently no uplink data transmission occurred:

³Notice that the time resource for $\xi_{\text{csi}}^{(d)}$ is limited by T_c/S , while for $\xi_{\text{csi}}^{(u)}$ is limited by the overall transmission duration t . In fact, we assume in our analyses that the uplink pilot training phase is much shorter than the actual data transmission and ignore its impact on the information outage performance in Section IV.

energy outage $\mathcal{O}_i^{(d)}$, or ii) uplink transmission occurred but the transmitted message could not be decoded at the HAP: information outage $\mathcal{O}_i^{(u)}$. Since downlink and uplink channels are independent and transmit powers are fixed we have that s_i 's outage probability is given by

$$\begin{aligned} \mathcal{O}_i &= 1 - (1 - \mathcal{O}_i^{(d)})(1 - \mathcal{O}_i^{(u)}) \\ &= \mathcal{O}_i^{(d)} + \mathcal{O}_i^{(u)} - \mathcal{O}_i^{(d)}\mathcal{O}_i^{(u)}. \end{aligned} \quad (2)$$

Finally, the network performance is evaluated in terms of the worst node's performance by computing the network outage probability as

$$\mathcal{O} = \sup_{i=1, \dots, S} \{\mathcal{O}_i\}. \quad (3)$$

Then, we can assure that every EH device in the network performs reliably at least the $(1 - \mathcal{O})\%$ of time. Notice that for $\mathcal{O}_i \ll 1$, the term $\mathcal{O}_i^{(d)} + \mathcal{O}_i^{(u)}$ dominates (2). Consequently, and since $\mathcal{O}_i \ll 1$ is required in practical scenarios, we can examine independently the bounds on $\mathcal{O}_i^{(d)}$ and $\mathcal{O}_i^{(u)}$.

III. WIRELESS ENERGY TRANSFER

In Subsection III-A, we first propose a CSI-based precoding scheme for optimizing the WET process. Then, we address the CSI-free WET alternative in Subsection III-B. The energy outage performance under both CSI-based and CSI-free WET schemes is also analyzed therein.

A. CSI-based WET

In each coherence block time, the HAP sends pilot signals that are used by the EH devices to estimate the downlink channels. Then, such information is fed back to the HAP through the uplink channels in an ordered way. As commented before, in such processes, the EH devices spend $\xi_{\text{csi}}^{(d)}$ energy units each time, which is approximately given as

$$\xi_{\text{csi}}^{(d)} \approx M_t \xi_0, \quad (4)$$

where ξ_0 denotes the energy required for decoding, processing and sending back to the HAP the information related to the pilot signals coming from each antenna. As we will show later in Subsection III-A3, very often, the HAP only requires the WET-CSI from a small set of EH devices, and therefore it is expected that their CSI feedback can be scheduled without overlapping.

As there are M_t transmit antennas, the HAP is able to transmit M_t energy beams to broadcast energy to all sensors in \mathcal{S} . Then, the incident RF power at s_i is given by

$$\begin{aligned} E_i^{\text{rf}} &= \mathbb{E}_x \left[\left(\sqrt{P\beta_i} (\mathbf{h}_i^{(d)})^T \sum_{j=1}^{M_t} \mathbf{w}_j x_j \right)^H \left(\sqrt{P\beta_i} (\mathbf{h}_i^{(d)})^T \sum_{j=1}^{M_t} \mathbf{w}_j x_j \right) \right] \\ &= P\beta_i \sum_{j=1}^{M_t} |(\mathbf{h}_i^{(d)})^T \mathbf{w}_j|^2 \mathbb{E}[x_j^H x_j] \\ &= P\beta_i \sum_{j=1}^{M_t} |(\mathbf{h}_i^{(d)})^T \mathbf{w}_j|^2, \end{aligned} \quad (5)$$

where P is the HAP's transmit power, $\mathbf{w}_j \in \mathbb{C}^{M_t \times 1}$, $j = 1, \dots, M_t$, denotes the precoding vector for generating the j -th energy beam, and x_j is its normalized energy carrying signal, i.e., $\mathbb{E}[x_j^H x_j] = 1$, which is independently generated across the antennas, i.e., $\mathbb{E}[x_j^H x_l] = 0$, $\forall j \neq l$.

For our setup and performance evaluation criterion, the optimum precoder $\{\mathbf{w}_j\}$ is the one that minimizes $\sup_{i=1, \dots, S} \{\mathcal{O}_i^{(d)}\}$. However, since the set $\{h_i^{(d)}\}$ is known by the HAP after the CSI acquisition procedures, the problem translates to maximize $\inf_{i=1, \dots, S} \{E_i^{\text{rf}}\}$ subject to $\sum_{j=1}^{M_t} \|\mathbf{w}_j\|^2 \leq 1$. The previous objective function is not concave and therefore the problem is not convex. However, it can still be optimally solved by rewriting it as a semi-definite programming (SDP) problem [27], as shown next.

1) *Energy beamforming*: First, define $\zeta \triangleq \inf_i \{E_i^{\text{rf}}\}$, while E_i^{rf} in (5) can be rewritten as

$$E_i^{\text{rf}} = P\beta_i \sum_{j=1}^{M_t} \mathbf{h}_i^{(d)H} \mathbf{w}_j \mathbf{w}_j^H \mathbf{h}_i^{(d)} = P\beta_i \text{Tr}(\mathbf{W} \mathbf{H}_i^{(d)}), \quad (6)$$

where $\mathbf{W} = \sum_{j=1}^{M_t} \mathbf{w}_j \mathbf{w}_j^H$ and $\mathbf{H}_i^{(d)} = \mathbf{h}_i^{(d)} \mathbf{h}_i^{(d)H}$. Second, notice that \mathbf{W} is a Hermitian matrix (with maximum rank $\min(S, M_t)$) that can be found by solving

$$\mathbf{P} : \underset{\mathbf{W} \in \mathbb{C}^{M_t \times M_t}, \zeta}{\text{minimize}} \quad -\zeta \quad (7a)$$

$$\text{subject to} \quad P\beta_i \text{Tr}(\mathbf{W} \mathbf{H}_i^{(d)}) \geq \zeta, \quad i=1, \dots, S \quad (7b)$$

$$\text{Tr}(\mathbf{W}) = 1 \quad (7c)$$

$$\mathbf{W} \succeq 0, \quad (7d)$$

which is an SDP problem. Notice that (7c) corresponds to the power budget constraint. Finally, the beamforming vectors $\{\mathbf{w}_j\}$ match the eigenvectors of \mathbf{W} but normalized by their corresponding eigenvalues' square roots such that $\text{Tr}(\mathbf{W}) = 1$. This procedure allows finding the optimum precoding vectors, and hereinafter it is referred to as CSI-based beamforming.

Interior point methods are mostly adopted to efficiently solve SDP problems. Since \mathbf{P} consists of a linear function, $S+1$ linear constraints, one positive semi-definite constraint, and the more challenging optimization variable has size $M_t \times M_t$, interior point methods will take $\mathcal{O}(M_t \log(1/\epsilon))$ iterations, with each iteration requiring at most $\mathcal{O}(M_t^6 + (S+1)M_t^2)$ arithmetic operations [28], where ϵ represents the solution accuracy at the algorithm's termination. In addition, an eigendecomposition of \mathbf{W} , which has complexity $\mathcal{O}(M_t^3)$, is required in order to derive the set of beamforming vectors. Consequently, the SDP solution becomes computationally costly as the number of PB's antennas and/or the number of EH devices increases.

2) *Energy outage lower bound*: Notice that

$$\sup_i \{\mathcal{O}_i^{(d)}\} \geq \inf_{\{\mathbf{w}_j\}, \forall j} \{\mathcal{O}_{i'}^{(d)}\}, \quad (8)$$

where $s_{i'}$ is the sensor under the greatest path loss: $\beta_{i'} \leq \beta_i$, $\forall s_i \in \mathcal{S}$, e.g., the farthest sensor. The above expression strictly holds as long as we consider the same energy requirements for all devices, e.g., homogeneous devices with the same transmit power $p_i = p$, $\forall s_i \in \mathcal{S}$. However, (8) should also hold when intelligent power allocation policies are utilized.

In the best possible scenario, where the HAP requires compensating only the channel impairments of $s_{i'}$ since the remaining nodes are under much better favorable channel/propagation conditions, a MRT precoding will be the optimum. Such MRT precoding is indistinctly and equivalently given by

$$\mathbf{w}_j = \frac{1}{\sqrt{M_t}} \frac{\mathbf{h}_{i'}^{(d)*}}{\|\mathbf{h}_{i'}^{(d)}\|}, \quad \forall j, \quad \text{or} \quad \begin{cases} \frac{\mathbf{h}_{i'}^{(d)*}}{\|\mathbf{h}_{i'}^{(d)}\|}, & j = 1 \\ \mathbf{0}, & j > 1 \end{cases}, \quad (9)$$

for which $E_{i'}^{\text{rf}}$ in each coherence interval becomes

$$E_{i'}^{\text{rf}} = P\beta_{i'} \|\mathbf{h}_{i'}^{(d)}\|^2 \sim \frac{P\beta_{i'}}{2(1+\kappa)} \mathfrak{X}, \quad (10)$$

which comes from using [20, Eq. (45)] and setting $\mathfrak{X} \sim \chi^2(2M_t, 2M_t\kappa)$.

We assume that the energy harvested between consecutive uplink transmissions requires to be enough for powering the circuits, performing the CSI acquisition procedures, and sending an uplink information message, while the remaining (if any) energy is used in other tasks, e.g., sensing, signal processing, etc. Therefore,

- for periodic traffic, the total energy harvested by $s_{i'}$ between its uplink transmissions is at most given by

$$E_{i'} \stackrel{(a)}{=} \eta T_c \sum_{\lceil t_s/T_c \rceil} E_{i'}^{\text{rf}} \stackrel{(b)}{\approx} \frac{\eta T_c P \beta_i}{2(1+\kappa)} \sum_{\lceil t_s/T_c \rceil} \mathfrak{X} \stackrel{(c)}{\approx} \frac{\eta T_c P \beta_i}{2(1+\kappa)} \chi^2(2M_t \lceil t_s/T_c \rceil, 2M_t \kappa \lceil t_s/T_c \rceil), \quad (11)$$

where in (a), $\eta \in (0, 1)$ denotes the energy conversion efficiency, and the summation is over $\lceil t_s/T_c \rceil$ independent RVs of the form of $E_{i'}^{\text{rf}}$, (b) comes from using (10), while (c) follows after using the definition of a non-central chi-square RV. Notice that although we conveniently used $\lceil t_s/T_c \rceil$ to take advantage of a finite summation, the last expression holds without such a constraint.

Meanwhile, the energy requirements under periodic traffic are given by

$$E_0 = \left\lceil \frac{t_s}{T_c} \right\rceil \xi_{\text{csi}}^{(d)} + \xi_{\text{csi}}^{(u)} + p_c t_s + pt, \quad (12)$$

thus (8) becomes

$$\begin{aligned} \sup_i \{\mathcal{O}_i^{(d)}\} &\geq \mathbb{P}[E_{i'} < E_0] \\ &\geq 1 - \mathcal{Q}_{M_t \lceil \frac{t_s}{T_c} \rceil} \left(\sqrt{2M_t \kappa \lceil \frac{t_s}{T_c} \rceil}, \sqrt{2(1+\kappa)} \times \right. \\ &\quad \left. \times \sqrt{\frac{\lceil \frac{t_s}{T_c} \rceil \xi_{\text{csi}}^{(d)} + \xi_{\text{csi}}^{(u)} + p_c t_s + pt}{\eta T_c P \beta_{i'}}} \right), \quad (13) \end{aligned}$$

which comes from using the CDF of a non-central chi-square RV; while

- for Poisson traffic, the messages arrive with an exponential inter-arrival random time U with mean $1/\lambda$ (given in coherence intervals). For analytical tractability, let us assume that transmissions also occur in an slotted fashion, where slots are of duration t . Then, devices with

a ready-to-send message wait for the next time slot for transmission.

Let us denote the inter-arrival RV by V , which is non-discrete and with PMF given by

$$\begin{aligned} \mathbb{P}[V = v] &= \mathbb{P}[v - 1 \leq U < v] \\ &= F_U(v) - F_U(v - 1) = (e^\lambda - 1)e^{-\lambda v} \end{aligned} \quad (14)$$

for $v \geq 1$. Now, $E_{i'}$ becomes a random sum of $E_{i'}^{\text{rf}}$ RVs; i.e., $E_{i'} = \eta T_c \sum_V E_{i'}^{\text{rf}}$, while the energy requirement to make the uplink transmissions take place are random as well, and can be written as

$$E_0 = v\xi_{\text{csi}}^{(d)} + \xi_{\text{csi}}^{(u)} + p_c v T_c + pt. \quad (15)$$

Then

$$\begin{aligned} \sup_i \{\mathcal{O}_i^{(d)}\} &\geq \mathbb{P}[E_{i'} < E_0] \\ &= \mathbb{P}\left[\eta T_c \sum_V E_{i'}^{\text{rf}} < v\xi_{\text{csi}}^{(d)} + \xi_{\text{csi}}^{(u)} + p_c v T_c + pt\right] \\ &\stackrel{(a)}{=} \mathbb{E}_V \left[\mathbb{P}\left[\frac{\eta T_c P \beta_{i'}}{2(1 + \kappa)} \sum_V \mathfrak{X} < v\xi_{\text{csi}}^{(d)} + \xi_{\text{csi}}^{(u)} + p_c v T_c + pt \mid V\right] \right] \\ &\stackrel{(b)}{=} 1 - \mathbb{E}_V \left[\mathcal{Q}_{M_t v} \left(\sqrt{2M_t \kappa v}, \sqrt{\frac{2(1 + \kappa)}{\eta T_c P \beta_{i'}}} \times \sqrt{v(\xi_{\text{csi}}^{(d)} + p_c T_c) + \xi_{\text{csi}}^{(u)} + pt} \right) \right] \\ &\stackrel{(c)}{\approx} 1 - (e^\lambda - 1) \sum_{v=1}^{v_{\max}} \mathcal{Q}_{M_t v} \left(\sqrt{2M_t \kappa v}, \frac{2(1 + \kappa)}{\eta T_c P \beta_{i'}} \times \sqrt{v(\xi_{\text{csi}}^{(d)} + p_c T_c) + \xi_{\text{csi}}^{(u)} + pt} \right) e^{-\lambda v}, \end{aligned} \quad (16)$$

where (a) comes from averaging the outage events conditioned on a given v and using (10), while (b) follows by taking the summation of v non-central chi-squared RVs, which obeys a non-central chi-squared distribution as well, but with v times the number of degrees of freedom and non-centrality parameter, and using its CDF by taking advantage of (1), while (c) follows after taking the expectation with respect to V by using (14). Notice that we avoided using an infinite notation in the last step, and instead considered only the first v_{\max} summands, hence (16) is, in general, an approximation that becomes exact as $v_{\max} \rightarrow \infty$. However, since V is a discrete exponential-like random variable characterized in (14), setting v_{\max} such that $v_{\max} \geq 10 \times \mathbb{E}[V]$ is enough for a good accuracy. Notice that

$$\mathbb{E}[V] = \frac{e^\lambda}{e^\lambda - 1}, \quad (17)$$

which follows from realizing that computing $\mathbb{E}[V] = \sum_{v=1}^{\infty} v e^{-\lambda v}$ is equivalent to evaluate e^λ into the Z -transform of the sequence $1, 2, 3, \dots$, which is $\frac{z^{-1}}{(1-z^{-1})^2}$.

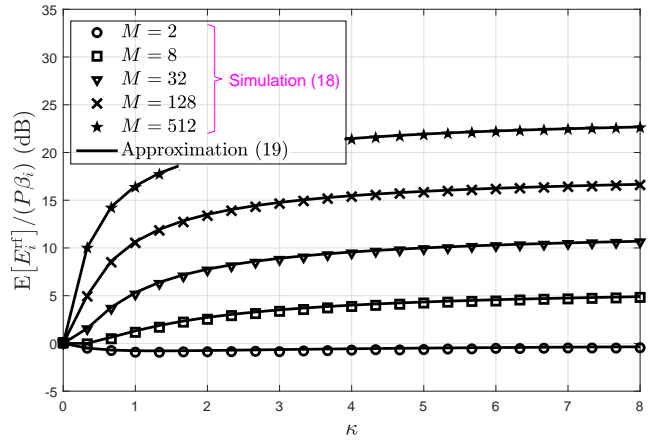


Fig. 2. $\mathbb{E}[E_i^{\text{rf}}]/(P\beta_i)$ vs κ for $M_t \in \{2, 8, 32, 128, 512\}$. Comparison between the Monte Carlo-based (18) and the analytical approximation (19).

3) *On the optimality of the MRT beamforming:* Let us assume that the HAP is using the MRT beamformer to power the farthest node $s_{i'}$. One question arises: *How such beamformer impacts the wireless powering of the remaining devices?* To shed some light into that matter, let us focus on the performance in terms of average incident RF power in a certain device $s_i \in \mathcal{S} \setminus s_{i'}$. By using (5) and the second MRT beamformer given in (9), we have that

$$\begin{aligned} \mathbb{E}[E_i^{\text{rf}}] &= \mathbb{E}\left[P\beta_i \sum_{j=1}^{M_t} |(\mathbf{h}_i^{(d)})^T \mathbf{w}_j|^2\right] \\ &= P\beta_i \mathbb{E}\left[|(\mathbf{h}_i^{(d)})^T \mathbf{w}_1|^2\right] \\ &= P\beta_i \mathbb{E}\left[\frac{|\mathbf{h}_{i'}^{(d)H} \mathbf{h}_i^{(d)}|^2}{\|\mathbf{h}_{i'}^{(d)}\|^2}\right]. \end{aligned} \quad (18)$$

Unfortunately, \mathbf{w}_1 follows a cumbersome projected normal distribution when $\mathfrak{S}\{\mathbf{w}_1\} = \mathbf{0}$ [29], which makes the analysis of the distribution of $|(\mathbf{h}_i^{(d)})^T \mathbf{w}_1|^2$ already very complicated even for such a simplified scenario. Meanwhile, decoupling the expression as shown in the last line of (18) does not solve the problem since numerator and denominator are correlated. We resorted to simulation and standard fitting procedures, and found out that

$$\frac{\mathbb{E}[E_i^{\text{rf}}]}{P\beta_i} \approx \frac{1}{4} \left(\frac{\kappa}{1 + \kappa/\sqrt{2}} \right)^2 M_t + \frac{1}{1 + \kappa/2} \quad (19)$$

matches (18) accurately, which is corroborated in Fig. 2. Now, notice that based on (10), we have that

$$\mathbb{E}[E_{i'}^{\text{rf}}] = P\beta_{i'} M_t, \quad (20)$$

thus,

$$\frac{\mathbb{E}[E_i^{\text{rf}}]}{\mathbb{E}[E_{i'}^{\text{rf}}]} \approx \frac{\beta_i}{\beta_{i'}} \left(\frac{1}{4} \left(\frac{\kappa}{1 + \kappa/\sqrt{2}} \right)^2 + \frac{1}{M_t(1 + \kappa/2)} \right). \quad (21)$$

When $\mathbb{E}[E_i^{\text{rf}}]/\mathbb{E}[E_{i'}^{\text{rf}}] > 1, \forall i : s_i \in \mathcal{S} \setminus s_{i'}$, we have that even when the HAP uses only the CSI statistics referred to $s_{i'}$, the remaining devices harvest more energy at least on average. In such scenario the MRT beamformer is most of the

TABLE I
MAIN SYSTEM PERFORMANCE CHARACTERISTICS UNDER THE CONSIDERED CSI-BASED AND CSI-FREE WET SCHEMES

Schemes	No. Tx. Antennas	Average EH Gain	EH Diversity	No. Rx. Antennas	Energy Requirements
CSI-based	M_t	$\leq M_t$	M_t	$M - M_t$	Moderate–High
CSI-free (SA)	1	1	M	$M - 1$	Low–Moderate

time the optimum from a system perspective. Now notice that if we consider the large-LOS scenario, (21) simplifies to

$$\frac{\mathbb{E}[E_{i'}^{\text{rf}}]}{\mathbb{E}[E_{i'}^{\text{rf}}]} \stackrel{\kappa \rightarrow \infty}{\approx} \frac{\beta_i}{2\beta_{i'}}, \quad (22)$$

which basically tells us that when $s_{i'}$ undergoes a path-loss at least 3dB greater than the experienced by the remaining EH nodes, the optimum energy beamformer is given by (9) most of the time.

B. CSI-free WET

Several CSI-free powering schemes have been recently proposed and analyzed in [20], [21], e.g., OA, AA – SS, AA – IS and SA. In Section I, we highlighted their main characteristics and argued why we adopt the SA scheme as our CSI-free scheme in this paper. Summarizing, the reasons are three-fold: i) among the schemes taking advantages of the spatial resources, SA exhibits a homogeneous performance over the space, which is not sensitive to the different mean phases of the LOS channel component; ii) it is more suitable than the AA – IS scheme for powering devices far from the HAP; and iii) it allows a better coupling to the co-located information transmission processes since only one antenna may be transferring energy in the downlink while the remaining may be receiving uplink information.

In our setup, the adoption of the SA scheme implies that each transmit antenna is active during T_c/M seconds, while the remaining $M - 1$ antennas function as receive antennas, i.e., $M_t = 1$, $M_r = M - 1$. The incident RF power at $s_{i'}$ is then given by

$$E_{i'}^{\text{rf}} = \frac{P\beta_{i'}}{M} \|\tilde{\mathbf{h}}_{i'}^{(d)}\|^2 \sim \frac{P\beta_{i'}}{2M(1 + \kappa)} \chi^2(2M, 2M\kappa), \quad (23)$$

which comes from exploring the connection to (10) and defining $\tilde{\mathbf{h}}_{i'}^{(d)} \in \mathbb{C}^{M \times 1}$ since all antennas transmit during a coherence block, although not simultaneously. Consequently, by taking $\xi_{\text{csi}}^{(d)} \leftarrow 0$, $P \leftarrow P/M$ and $M_t \leftarrow M$ the energy outage bounds given in (13) and (16) for periodic and Poisson traffic, respectively, hold here as well. Notice that under the CSI-based scheme, the average harvested energy can be up to M times greater than under SA scheme, for which $\mathbb{E}[E_{i'}^{\text{rf}}] = P\beta_{i'}$, however, the diversity gain of SA is $M/M_t^{\text{mrt}} > 1$ greater since all antennas contribute.

A summary on the system performance characteristics under the CSI-based and CSI-free WET schemes is presented in Table I. Notice that the average EH gain is counted as $\mathbb{E}[E_{i'}^{\text{rf}}]/(P\beta_{i'})$, while the energy requirement field accounts for all energy consumption sources including the uplink CSI-acquisition procedure which is required for both analyzed schemes.

IV. WIRELESS INFORMATION TRANSMISSION

As commented in Section II, at some points, the EH devices require sending short data messages of k bits/Hz over blocks of t seconds to the HAP. The HAP utilizes M_r antennas to decode the arriving messages and resolve possible simultaneous transmissions. Uplink CSI is required to implement the ZF or MMSE linear decoding schemes which we adopt here, while the analysis under non-coherent decoding schemes is left for future work.

Notice that we consider an uninterrupted downlink WET, while now and then a subset of the devices interrupt their harvesting process to send uplink data. The self-interfering powering signals, traveling through the channels between the M_t transmit antennas and M_r receive antennas are assumed to be perfectly canceled via Successive Interference Cancellation (SIC) techniques, which may include analog and digital processes. Such SIC techniques can benefit from the fact that the powering signals can be chosen deterministically.

Finally, under the SA scheme we assume that the transmit slots are scheduled such that no antenna switching occurs during an actual uplink transmission, which would complicate the information decoding procedures. Next, we analyze the WIT performance under the considered traffic profiles.

A. WIT under periodic traffic

As commented in Subsection II-B the maximum number of concurrent transmissions is deterministically $\lceil S/[t_s/t] \rceil$, thus, the HAP requires that same number of orthogonal pilot signals and consequently pilot symbols. Then, under periodic traffic, $\xi_{\text{csi}}^{(u)}$ can be broken approximately into

$$\xi_{\text{csi}}^{(u)} \approx \lceil S/[t_s/t] \rceil \tilde{\xi}_0, \quad (24)$$

where $\tilde{\xi}_0$ is the per-symbol pilot energy. Next, we investigate the outage performance of the data transmission phase.

1) *Signal model*: At the HAP, the data signal received after each transmission is given by

$$\mathbf{y} = \mathbf{H}^{(u)} \mathbf{P}_\beta^{1/2} \mathbf{x} + \mathbf{w}, \quad (25)$$

where the j -th column of $\mathbf{H}^{(u)}$ is $\mathbf{h}_j^{(u)}$ and consequently such matrix has dimension $M_r \times S$, $\mathbf{P}_\beta = \text{diag}(\{p_i\beta_i\})$, $\mathbf{x} \in \mathbb{C}^{S \times 1}$ is the normalized vector of the normal signals transmitted by the S devices, and $\mathbf{w} \sim \mathcal{CN}(\mathbf{0}, \sigma^2 \mathbf{I}_{M_r \times M_r})$ is the Additive White Gaussian Noise (AWGN) vector at the M_r antennas. If s_i is not active in a given transmission slot of duration t , we consider that the respective entries in $\mathbf{H}^{(u)}$, \mathbf{P}_β and \mathbf{x} are zero. Consequently the number of non-zero columns of $\mathbf{H}^{(u)}$ is at most $\lceil S/[t_s/t] \rceil$, which matches also the maximum number of non-zero rows and columns of \mathbf{P}_β , and the number of non-zero elements of \mathbf{x} . Finally, the equalizer $\mathbf{Q} \in \mathbb{C}^{M_r \times M_r}$ at

the receiver decouples the transmitted data streams such that its output is given by

$$\mathbf{y}_{\text{out}} = \mathbf{Q}\mathbf{y} = \mathbf{Q}\mathbf{H}^{(u)}\mathbf{P}_\beta^{1/2}\mathbf{x} + \mathbf{Q}\mathbf{w}. \quad (26)$$

2) *ZF*: The ZF equalizer is

$$\begin{aligned} \mathbf{Q}^{\text{zf}} &= \left((\mathbf{H}^{(u)}\mathbf{P}_\beta^{1/2})^H \mathbf{H}^{(u)}\mathbf{P}_\beta^{1/2} \right)^{-1} (\mathbf{H}^{(u)}\mathbf{P}_\beta^{1/2})^H \\ &= \mathbf{P}_\beta^{-1/2} \left(\mathbf{H}^{(u)H} \mathbf{H}^{(u)} \right)^{-1} \mathbf{H}^{(u)H}, \end{aligned} \quad (27)$$

and by substituting it into (26) yields

$$\mathbf{y}_{\text{out}}^{\text{zf}} = \mathbf{x} + \mathbf{P}_\beta^{-1/2} \left(\mathbf{H}^{(u)H} \mathbf{H}^{(u)} \right)^{-1} \mathbf{H}^{(u)H} \mathbf{w}. \quad (28)$$

Then, the instantaneous Signal to Interference-plus-Noise Ratio (SINR) of the output stream corresponding to the one transmitted by s_i is given by

$$\begin{aligned} \gamma_i^{\text{zf}} &= \frac{1}{\left[\left((\mathbf{H}^{(u)}\mathbf{P}_\beta^{1/2})^H \mathbf{H}^{(u)}\mathbf{P}_\beta^{1/2} \right)^{-1} \right]_{i,i} \sigma^2} \\ &= \frac{1}{\left[\mathbf{P}_\beta^{-1/2} \left(\mathbf{H}^{(u)H} \mathbf{H}^{(u)} \right)^{-1} \mathbf{P}_\beta^{-1/2} \right]_{i,i} \sigma^2} \\ &= \frac{1}{\left[\mathbf{P}_\beta^{-1/2} \mathbf{Z} \mathbf{P}_\beta^{-1/2} \right]_{i,i} \sigma^2} = \frac{p_i \beta_i}{\sigma^2} Z^{\text{zf}}, \end{aligned} \quad (29)$$

where $Z^{\text{zf}} = 1/Z_{i,i}$ with $\mathbf{Z} = (\mathbf{H}^{(u)H} \mathbf{H}^{(u)})^{-1}$. For Rayleigh fading, i.e., $\kappa = 0$, \mathbf{Z} has the central inverse Wishart distribution, which for the case of M_r greater than the number of data streams N , yields to $Z^{\text{zf}} \sim 2\chi^2(2(M_r - N + 1))$. Meanwhile, the analysis under Rician fading is encumbered by the noncentrality of the Wishart distribution of \mathbf{Z}^{-1} . The usual approach in such case lies in approximating the noncentral Wishart distribution by the virtual central Wishart distribution as summarized in [30]. In any case, the analysis is cumbersome, specially for the general scenario where $M_r \geq N$ does not need to necessarily hold, thus, we take no further steps to characterize the distribution of Z^{zf} . Whenever the statistics of Z^{zf} are required, we use a Monte Carlo-based approach.

3) *MMSE*: The MMSE equalizer is

$$\mathbf{Q}^{\text{mmse}} = \left(\mathbf{P}_\beta^{1/2} \mathbf{H}^{(u)H} \mathbf{H}^{(u)} \mathbf{P}_\beta^{1/2} + \sigma^2 \mathbf{I} \right)^{-1} (\mathbf{H}^{(u)} \mathbf{P}_\beta^{1/2})^H, \quad (30)$$

while the corresponding component for decoding the i -th data stream is given by

$$\mathbf{q}_i^{\text{mmse}} = \left(\sigma^2 \mathbf{I} + \sum_{j \neq i}^S \beta_j p_j \mathbf{h}_j^{(u)} \mathbf{h}_j^{(u)H} \right)^{-1} \mathbf{h}_i^{(u)}. \quad (31)$$

Then, the corresponding instantaneous SINR is given by

$$\gamma_i^{\text{mmse}} = \frac{\beta_i p_i}{\sigma^2} Z^{\text{mmse}}, \quad (32)$$

where $Z^{\text{mmse}} = \mathbf{h}_i^{(u)H} \left(\mathbf{I} + \sum_{j \neq i}^S \frac{\beta_j p_j}{\sigma^2} \mathbf{h}_j^{(u)} \mathbf{h}_j^{(u)H} \right)^{-1} \mathbf{h}_i^{(u)}$. Even for the simplest scenario with Rayleigh fading, equal per-user SNR, and $M_r \geq N$, the distribution of Z^{mmse} is cumbersome as corroborated in [31], [32]. This, and the fact that for a more general scenario there is no closed-form expression for the PDF and CDF of Z^{mmse} , we rely again on Monte Carlo simulations whenever its statistics are required.

4) *Information outage performance*: For the sake of fairness, we assume that those devices with the most similar path losses are scheduled for concurrent transmission. This is possible under periodic traffic, which is deterministic by nature. Let us sort the devices according to their path loss such that s_1 is the device with the smallest attenuation, while $s_S = s_{i'}$ is the device under the greatest path loss. Now, we evaluate the information outage performance at $s_{i'}$ in order to get a bound on the performance of any node in the network⁴. Thus, we have that $N = \lceil S/\lfloor t_s/t \rfloor \rceil$, while (25) and subsequent derivations can be compacted by eliminating the zero-rows/columns of $\mathbf{H}^{(u)}$, \mathbf{P}_β , e.g. $\mathbf{H}^{(u)} \in \mathbb{C}^{M_r \times N}$, $\mathbf{P}_\beta = \text{diag}(\{p_i \beta_i\})$, $i = S - N + 1, \dots, S$, and reducing the dimension of vector \mathbf{x} , i.e., $\mathbf{x} \in \mathbb{C}^{N \times 1}$. Then,

$$\begin{aligned} \sup_i \{\mathcal{O}_i^{(u)}\} &\simeq \mathcal{O}_{i'}^{(u)} = \mathbb{P}[\log_2(1 + \gamma_{i'}) < k/t] = \mathbb{P}[\gamma_{i'} < 2^{k/t} - 1] \\ &= F_Z \left(\frac{(2^{k/t} - 1)\sigma^2}{\beta_{i'} p_{i'}} \right), \end{aligned} \quad (33)$$

which comes from using (29) and (32) such that $Z \in \{Z^{\text{zf}}, Z^{\text{mmse}}\}$.

B. WIT under Poisson traffic

Concurrent transmissions happen randomly under Poisson traffic. Therefore, there is no way of completely avoiding the pilot collisions unless all devices are allocated orthogonal pilot sequence. However, this can be extremely energy-costly for large S since $\xi_{\text{csi}}^{(u)} = S\tilde{\xi}_0$, where $\tilde{\xi}_0$ was defined in the previous subsection. To overcome this, we herein allow collisions to occur with a probability not greater than ε , which is a system parameter to be efficiently designed.

1) *Collision probability*: The probability that a given device s_i is active at a certain time slot is given by

$$\mathbb{P}[s_i \in \tilde{\mathcal{S}}] = \frac{1}{\mathbb{E}_V[vT_c/t]} = \frac{t/T_c}{\mathbb{E}_V[v]} = \frac{t}{T_c} (1 - e^{-\lambda}), \quad (34)$$

where $\tilde{\mathcal{S}} \subseteq \mathcal{S}$ denotes the set of active devices in such a time slot, and the last equality comes from using (17). Notice that the subset $\tilde{\mathcal{S}} \subseteq \mathcal{S}$ of active devices is random under Poisson traffic, and also its cardinality $N = |\tilde{\mathcal{S}}|$. Meanwhile, N is a Binomial RV with parameters S and $\frac{t}{T_c}(1 - e^{-\lambda})$ such that

$$\mathbb{P}[N = n] = \binom{S}{n} \left(\frac{t}{T_c} (1 - e^{-\lambda}) \right)^n \left(1 - \frac{t}{T_c} (1 - e^{-\lambda}) \right)^{S-n}$$

and $\mathbb{E}[N] = \frac{tS}{T_c} (1 - e^{-\lambda})$, which represents the average number of concurrent transmissions.

Now, let us take L as the number of orthogonal pilot sequences/symbols such that L/S is the pilot reuse factor, and denote as $\hat{\mathcal{S}} \subseteq \tilde{\mathcal{S}}$, where $N' = |\hat{\mathcal{S}}|$, the set of devices using the same pilot signal, then

$$\mathbb{P}[s_i \in \hat{\mathcal{S}}] = \frac{1}{L} \mathbb{P}[s_i \in \tilde{\mathcal{S}}] = \frac{t}{LT_c} (1 - e^{-\lambda}), \quad (35)$$

⁴Such bound is expected to hold under the assumption of equal devices' transmit power, or a power allocation such that a greater attenuation implies a smaller transmit power. While the latter seems odd at first sight since the farthest node is usually allowed to transmit with greater power in traditional cellular networks, it is not the case in WPCNs where the farthest device harvests also less energy.

and similarly N' is a Binomial RV with parameters S and $\frac{t}{LT_c}(1-e^{-\lambda})$. Consequently, $\mathbb{E}[N'] = \frac{St}{LT_c}(1-e^{-\lambda})$ represents the average number of concurrent transmissions of devices using the same pilot signals. As done previously, we focus attention to the performance of $s_{i'}$. Assuming such a device is already active, its associated collision probability is

$$\begin{aligned} \mathcal{O}_{\text{col}} &= 1 - \mathbb{P}[N' = 1 | N' > 0] = 1 - \frac{\mathbb{P}[N' = 1]}{1 - \mathbb{P}[N' = 0]} \\ &= 1 - \frac{\frac{St}{LT_c}(1-e^{-\lambda}) \left(1 - \frac{t}{LT_c}(1-e^{-\lambda})\right)^{S-1}}{1 - \left(1 - \frac{t}{LT_c}(1-e^{-\lambda})\right)^S}. \end{aligned} \quad (36)$$

Then, we must choose L such that $\mathcal{O}_{\text{col}} \leq \varepsilon$. However, notice that if such L is greater than S , it is preferable to deterministically assign one unique pilot sequence to each user, thus, avoiding the collisions completely. Therefore, the optimum L given ε is given by

$$L^* = \begin{cases} L_0, & \text{if } L_0 < S \rightarrow \mathcal{O}_{\text{col}} \text{ given in (36)} \\ S, & \text{otherwise} \rightarrow \mathcal{O}_{\text{col}} = 0 \end{cases}, \quad (37)$$

where

$$L_0 = \inf_{L \in \mathbb{Z}^+, \mathcal{O}_{\text{col}} \leq \varepsilon} L. \quad (38)$$

In the Appendix, we illustrate a simple procedure for solving (38). Finally,

$$\xi_{\text{csi}}^{(u)} = L^* \tilde{\xi}_0. \quad (39)$$

Next, we investigate the outage performance of the data transmission phase.

2) *Information outage performance:* Herein, we need to consider the pilot collision events and the outages due to decoding errors. Since \mathcal{O}_{col} takes into account the events related to the collided $s_{i'}$'s transmissions, we are now interested on the event where $s_{i'}$ operates without collision while the remaining IoT sensors in \tilde{S} may or may not be colliding. Consequently, we now have that

$$\begin{aligned} &\sup_i \{\mathcal{O}_i^{(u)}\} \\ &\stackrel{(a)}{\simeq} \mathcal{O}_{\text{col}} + (1 - \mathcal{O}_{\text{col}}) \mathbb{E}_{\tilde{S}|N \geq 1} \left[F_{Z|\tilde{S}, N \geq 1} \left(\frac{(2^{k/t} - 1)\sigma^2}{\beta_{i'} p_{i'}} \right) \right] \\ &\stackrel{(b)}{\simeq} \varepsilon + (1 - \varepsilon) \mathbb{E}_{\tilde{S}|N \geq 1} \left[F_{Z|\tilde{S}, N \geq 1} \left(\frac{(2^{k/t} - 1)\sigma^2}{\beta_{i'} p_{i'}} \right) \right]. \end{aligned} \quad (40)$$

The latter term in both (a) and (b) can be easily evaluated by

- 1) generating a sample N conditioned on $N \geq 1$;
- 2) drawing $N - 1$ elements from $S \setminus s_{i'}$ to conform the set of interfering devices;
- 3) evaluating (33) for such configuration;
- 4) averaging (33) over many possible realizations of N .

Finally, notice that setting the collision target probability ε for optimum system performance is a challenging task since the last term of (40) intricately depends on ε , hence, numerical analyses seem unavoidable and were carried out in the next section.

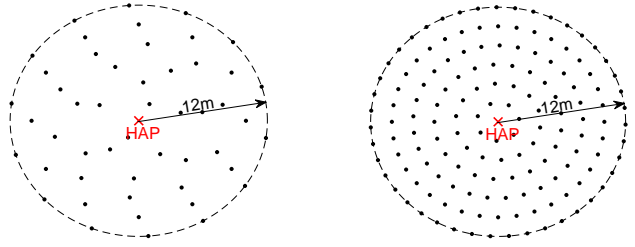


Fig. 3. Example deployments: (a) $S = 50$ (left) and (b) $S = 150$ (right).

V. NUMERICAL RESULTS

In this section, numerical examples are provided to corroborate our study and evaluate the suitability of the CSI-free or CSI-based WET schemes. We assume

$$\lambda = T_c/t_s$$

for a fair comparison between the periodic and Poisson traffic profiles. Also, the HAP has a maximum transmit power $P = 10\text{W}$, and its associated devices are distributed around in a 12m-radius circular area as shown in Fig. 3. Specifically, we consider the EH devices are at 2, 4, 6, 8, 10 and 12m from the HAP, while the number of devices in each sub-circumference is proportional to its length, thus, devices are approximately uniformly distributed in the coverage area. According to the adopted deployment scenario and the results and discussions in Subsection III-A3, around half of the EH devices (those at 10m and 12m from the HAP) are expected to fully determine the optimum EB most of the time. Consequently the HAP requires coordinating around $\sim S/2$ uplink transmissions for acquiring an effective downlink CSI of the network.

Channels remain static for $T_c = 400\text{ms}$, and are subject to a log-distance path-loss model with exponent 2.7 with non-distance dependent losses of 16dB. Thus, the average channel gain corresponding to the s_i 's uplink/downlink channels is given by

$$\beta_i = 10^{-1.6} \times d_i^{-2.7},$$

where d_i is the distance between s_i and the HAP. The noise power at the HAP's receive antennas is assumed to be $\sigma^2 = -94\text{dBm}$, and the EH efficiency, circuit power consumption and transmit power of the EH devices is set to $\eta = 0.25$, $20\mu\text{W}$ and $200\mu\text{W}$, respectively. Devices are required to transmit each message in the uplink within $t = 20\text{ms}$ time window ($M_0 = 20$ and we limit our analysis to $M \leq 20$). Additionally, unless stated otherwise, we set $S = 100$ to account for a massive deployment ($\sim 0.22\text{devices/m}^2$)⁵, $\kappa = 5$ to account for some LoS, and $k = 10^{-3}\text{bits/Hz}$ to account for low-rate transmissions as typical in MTC. Finally, $M = 6$, $t_s = 1.6\text{s}$, $\xi_0 = -20\text{dBm}$ and $\tilde{\xi}_0 = -30\text{dBm}$.

A. On the WET performance

Herein, we investigate the EH performance of the farthest node $s_{i'}$ under both CSI-free and CSI-based schemes. Such

⁵The projections towards 6G point to challenging scenarios with up to 10 devices/m² [2], [9], thus, the considered deployment is not as massive as it can be 10 years from now. Obviously, the larger the number of EH devices is, the more beneficial the analyzed CSI-free schemes are when compared to the traditional CSI-based schemes [20].

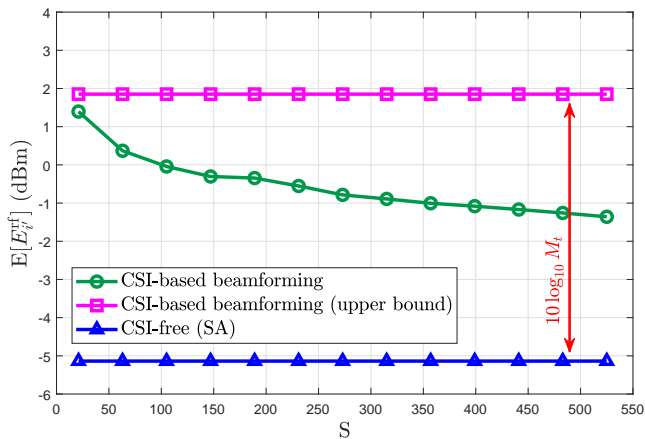


Fig. 4. Worst-case average harvested energy as a function of the number of EH devices. We set $M_t = 5$ for the CSI-based schemes.

node performs the worst in the network, thus, we can guarantee a minimum level performance for the entire set of devices. Fig. 4 shows the average RF energy availability as a function of the number of devices. Notice that the performance of the CSI-free SA scheme is independent of the number of devices, while the average RF energy under the CSI-based scheme decreases quickly as S increases. Obviously, only when $S \rightarrow \infty$, both SA and the CSI-based scheme converge to the same performance in terms of average RF energy supply. The best possible performance is when the farthest node is powered via a CSI-based MRT scheme, and still such node is sufficiently far such that it keeps performing the worst in the network. Therefore, a MRT under such circumstance provides an upper bound performance, which is always $10 \log_{10} M_t$ dB greater than SA's, as also illustrated in Fig. 4. From now on, we only show the results corresponding to the MRT bound since for the exact CSI-based performance, \mathbf{P} in (7) requires to be repeatedly solved, which is extremely costly. While the CSI-based scheme always outperforms the SA CSI-free scheme in terms of average RF energy supply, that is not longer the case when analyzing the EH performance in terms of energy outage probability. On one hand, the EH diversity is smaller in case of the CSI-based scheme as shown in Table I. On the other hand, the CSI-based scheme introduces additional sources of energy consumption, which is accounted in the term $\xi_{\text{csi}}^{(d)}$ and depends specifically on M_t and ξ_0 as stated in (4).

Fig. 5 shows the worst-case energy outage probability as a function of ξ_0 for both Poisson and periodic⁶ traffics when half of the antennas are used in downlink/uplink under the CSI-based scheme. The performance of the CSI-free SA scheme remains obviously constant, while the MRT gains from CSI disappear quickly as ξ_0 increases. However, notice that even when a greater M_t increases the CSI acquisition costs, it is still more advantageous than costly for the CSI-based scheme, since a greater M_t enlarges the ξ_0 region for which the CSI-based scheme is preferable. Finally, notice that under periodic traffic the performance is much better than when devices

⁶We used a much more restrictive circuit power consumption level in case of periodic traffic to better visualize the outage performance in a range of values that can be corroborated via Monte Carlo simulation. This was done only for Fig. 5.

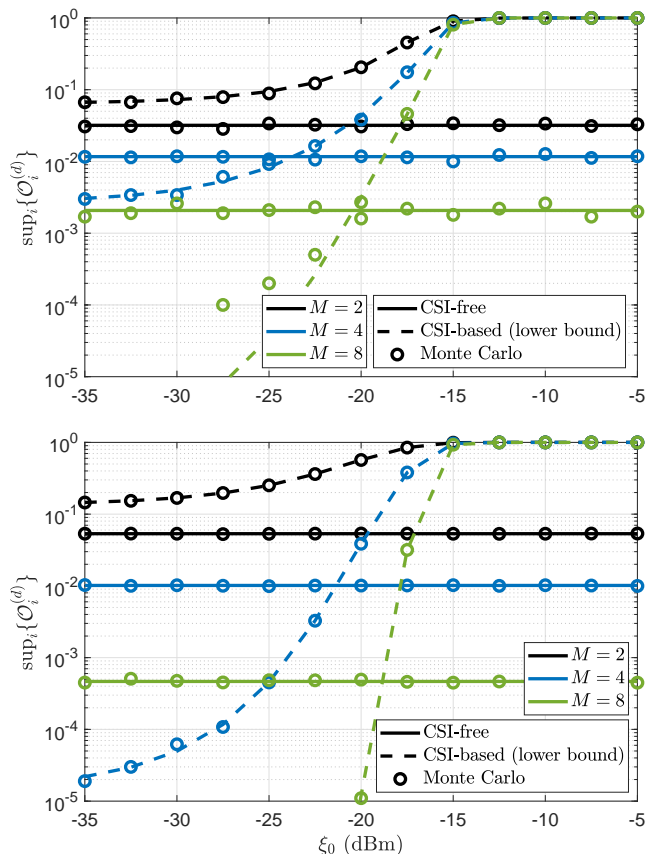


Fig. 5. Worst-case energy outage probability as a function of ξ_0 . a) Poisson traffic, $\varepsilon = 10^{-1}$, $p_c = 20 \mu\text{W}$ (top); and b) Periodic traffic, $p_c = 50 \mu\text{W}$. For the CSI-based schemes we set $M_t = M_r = M/2$ (bottom).

activate randomly according to a Poisson process.

B. On the WIT performance

Herein, we investigate the communication performance of the farthest node s_i when powered via either CSI-free or CSI-based WET schemes. We evaluate the worst-case information outage probability given a communication attempt. Specifically, Fig. 6 shows the performance degradation as the number of EH devices increases when the information decoding is done via MMSE and ZF techniques. In general, ZF is known to approach the MMSE performance at high SINR, but notice that here the MMSE scheme outperforms significantly the ZF scheme since the operation is at relatively small SINRs, because of the low-power low-rate transmissions. Therefore, operating under the MMSE decoding scheme is highly recommended, and hereinafter we only present the results related to MMSE. In case of Poisson traffic (Fig. 6a), the performance improves as ε decreases, since the collision probability decreases. However, as ε decreases, the changes of energy outage increase, which is not considered here, and may degrade the overall system performance as illustrated later in the next subsection. On the other hand, notice that as the number of receive antennas increases, the communication decoding capabilities improve considerably, which is illustrated for periodic traffic (Fig. 6b).

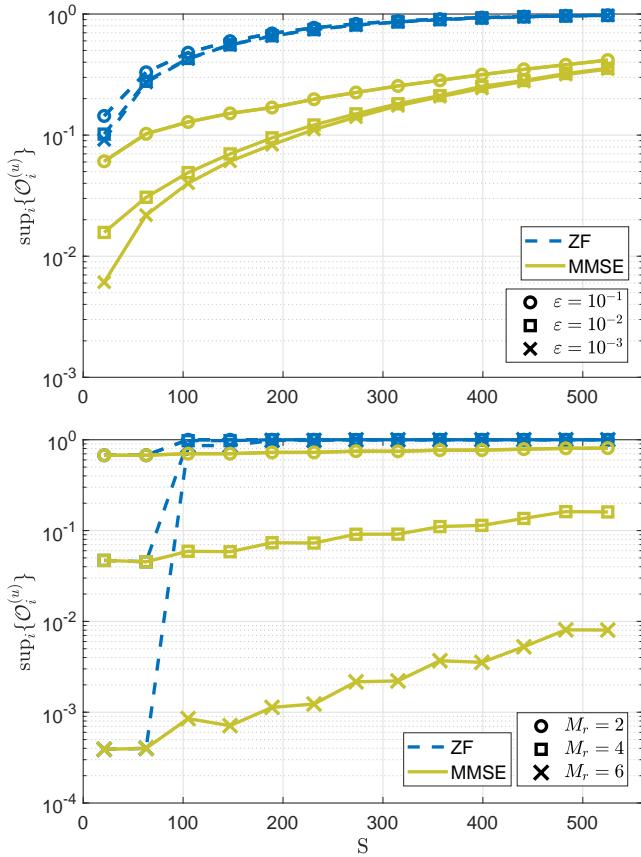


Fig. 6. Worst-case information outage probability as a function of the number of devices. *a*) Poisson traffic, $M_r = 4$, $\varepsilon \in \{10^{-1}, 10^{-2}, 10^{-3}\}$ (top); and *b*) Periodic traffic, $M_r \in \{2, 4, 6\}$ (bottom).

Fig. 7 shows the information outage as a function of the average number of coherence time intervals between the transmission of consecutive messages from each device (the periodicity in case of periodic traffic and the inverse of traffic rate in case of Poisson traffic). As such time increases, the performance improves since the number of concurrent transmissions decreases. In case of deterministic traffic, the maximum performance is attained when $N = 1$, which occurs when $t_s \geq 2s$, as corroborated in the figure. In case of Poisson traffic, the chances of no concurrent transmissions vanish only when $L^* = S$, which tends to happen as ε decreases and/or T_c/λ increases as shown in the figure. Once again, observe that periodic traffic patterns allow for a more reliable utilization of the spectrum resources.

C. On the general performance

Herein we investigate the overall outage performance by taking into consideration both the energy and information outage performances. As a first result and for a Poisson traffic scenario, we show in Fig. 8 the overall worst-case outage probability as a function of the collision target probability. In case of the CSI-based WET scheme, we utilize different antenna partitions and found out that the system benefits more by having no less receive antennas than transmit antennas. Anyway, the CSI-free SA scheme attains the best performance in all the cases shown. This means that the CSI acquisition

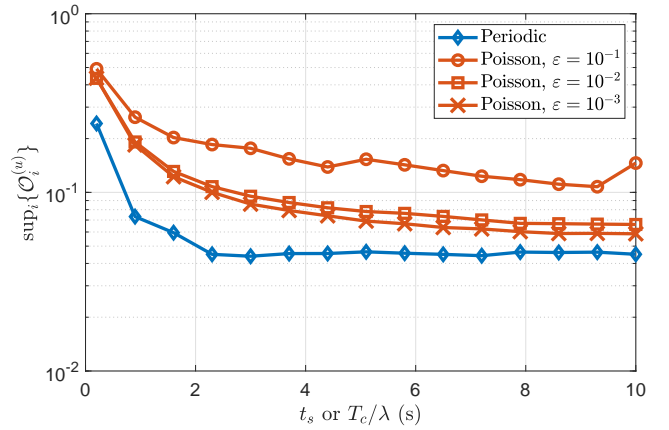


Fig. 7. Worst-case information outage probability as a function of the average number of coherence time intervals between the transmission of consecutive messages from each device. HAP uses MMSE and we set $M_r = 4$.

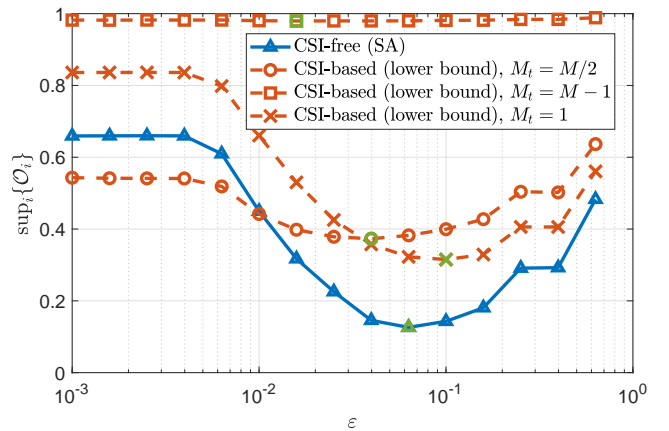


Fig. 8. Worst-case outage probability in a Poisson traffic scenario as a function of the collision target probability ε . We set $M = 6$.

costs overcame the beamforming gains. Besides, the main insight is that for each configuration there is an optimum collision target probability, which at the end influences significantly the overall system performance. Such optimum values are highlighted in green in the figure.

Fig. 9 shows the performance for both Poisson (Fig. 9a), with $\varepsilon \in \{10^{-1}, 10^{-2}\}$, and periodic (Fig. 9b) traffic as a function of the total number of antennas. In case of Poisson traffic, the performance highly depends on ε as commented in the previous paragraph, and corroborated now in Fig. 9a. One can see that the optimum ε is around 10^{-1} for $M \lesssim 8$, while a more stringent value should be adopted for $M \gtrsim 8$. Also, observe that for relatively small M , the CSI-free SA scheme is preferable, while as M increases, the CSI-based alternative becomes more suitable, specially by partitioning the set of transmit and receive antennas equally. In case of periodic traffic, the performance improvements as a function of M are even more noticeable. It is shown that, while having only one antenna dedicated to transmission is preferable for small M , there is need of a more equitable distribution of the transmit and receive antennas as M increases. Anyway, the CSI-free SA scheme outperforms all the CSI-based configurations in the examples illustrated in Fig. 9b.

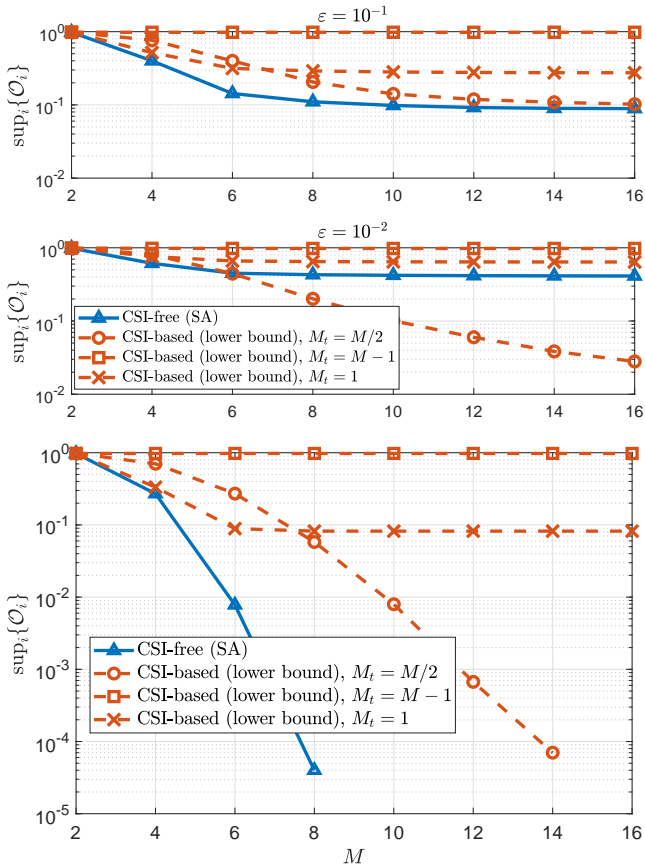


Fig. 9. Worst-case outage probability as a function of the number of antennas. *a*) Poisson traffic, $\varepsilon \in \{10^{-1}, 10^{-2}\}$ (top); and *b*) Periodic traffic (bottom).

The overall outage probability as a function of both transmit and receive CSI nominal acquisition costs, ξ_0 and $\tilde{\xi}_0$, respectively, is shown in Fig. 10a (Poisson traffic with $\varepsilon \in \{10^{-1}, 10^{-2}\}$) and Fig. 10b (periodic traffic). Notice that the SA scheme keeps a constant performance along the x -axis since the HAP does not require/use any CSI for powering the devices, while the performance under the CSI-based scheme is seriously affected as ξ_0 increases above -20 dBm. Meanwhile, the overall performance decreases as $\tilde{\xi}_0$ takes significant values since CSI is required for information decoding under both CSI-based and CSI-free WET mechanisms. This is accentuated under Poisson traffic whose performance is considerably inferior when compared to a periodic traffic scenario with the same average traffic characteristics. As observed, the CSI-free WET scheme is the most suitable under periodic traffic; while under Poisson traffic, it becomes attractive as $\tilde{\xi}_0$ decreases.

Fig. 11 shows the overall outage probability as a function of the average number of coherence time intervals between the transmission of consecutive messages from each device. As such average inter-arrival time increases, the chances of outage decrease. In case of Poisson traffic (Fig. 11a), the performance is strictly determined by the chosen collision probability target, whose optimum value tends to decrease as the average inter-arrival time increases. In case of periodic traffic (Fig. 11b), the overall performance improves, but bounded, with the inter-arrival time. The minimum outage probability is already reached for $t_s = 2s$, and this is due to the same arguments we

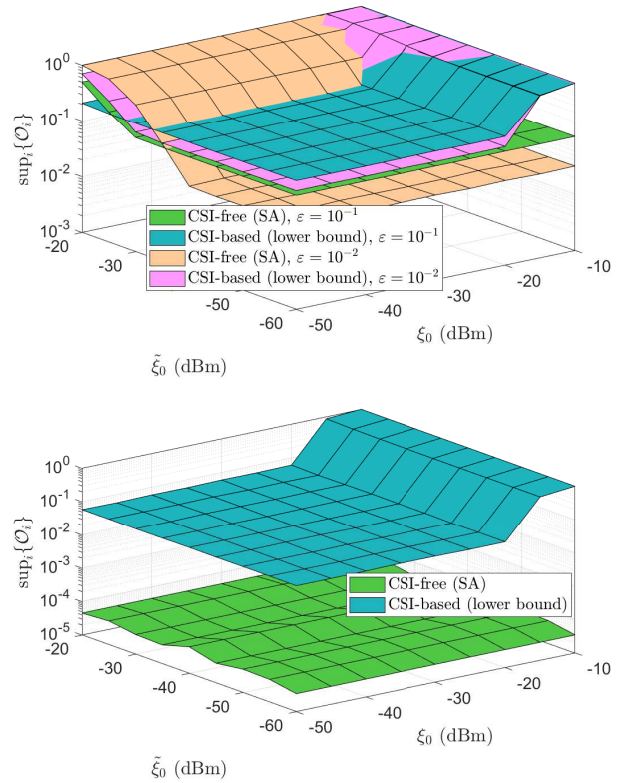


Fig. 10. Worst-case outage probability as a function of the CSI acquisition costs. *a*) Poisson traffic, $\varepsilon \in \{10^{-1}, 10^{-2}\}$ (top); and *b*) Periodic traffic (bottom).

exposed earlier when discussing Fig. 7 results. All the results in Fig. 11 show the benefits of operating without any CSI for WET.

VI. CONCLUSION

In this paper, we assessed for the first time the suitability of CSI-based and CSI-free multi-antenna WET schemes in a WPCN with a massive number of devices and under periodic or Poisson traffic sources. The system performance was evaluated, and optimized whenever possible, in terms of the worst (farthest) node's performance for the sake of fairness, and considering a realistic power consumption model at the devices. In case of the CSI-based WET scheme, we cast the optimization problem as an SDP problem, hence, a global solution is perfectly available by using regular optimization solvers. Additionally, we showed that a MRT beamformer is close to the optimum whenever the farthest node experiences at least 3 dB of power attenuation more than the remaining devices. As a CSI-free scheme, we adopted the novel SA strategy introduced and analyzed in [20], [21]. This scheme, although not capable of providing higher average harvesting gains compared to the CSI-based schemes, it does provide greater WET/WIT diversity gain with lower energy requirements. Our numerical results evidenced that the CSI-free scheme constitutes the optimum for most of the configurations. Although, its performance may degrade significantly if the setup is not optimally configured in case of Poisson traffic.

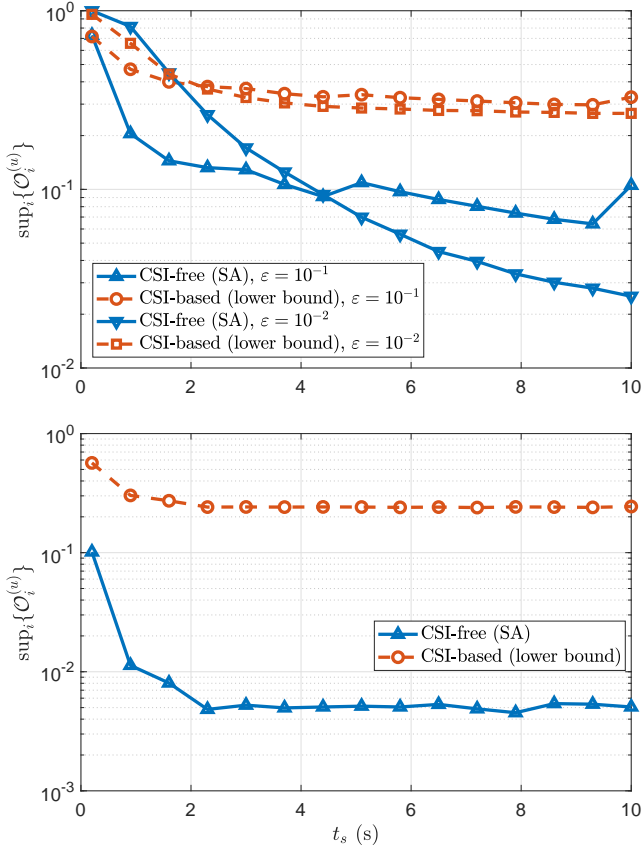


Fig. 11. Worst-case outage probability as a function of a) T_c/λ for Poisson traffic (top), b) t_s for periodic traffic. We set $M_t = M_r = M/2$ for the CSI-based schemes, while $M = 6$ (bottom).

In fact, the system performance not only deteriorates under Poisson random access when compared to deterministic traffic, but optimally configuring the network becomes also more challenging. In that regard, we cast an optimization problem to determine the optimum pilot reuse factor such that the collision probability under Poisson accesses remains below a certain limit. Numerical results demonstrated the existence of an optimum collision target probability. Finally, we showed the considerable gains from using a MMSE equalizer instead of a ZF equalizer in the analyzed WPCN scenario.

APPENDIX

Let us take

$$u = 1 - \frac{t}{LT_c}(1 - e^{-\lambda}), \quad (41)$$

then, by substituting (41) into (36), the problem in (38) can be easily addressed after solving for u the following inequality

$$\begin{aligned} \mathcal{O}_{\text{col}} &\leq \varepsilon \\ 1 - \frac{S(1-u)u^{S-1}}{1-u^S} &\leq \varepsilon \\ \frac{(1-u)u^{S-1}}{1-u^S} &\geq \frac{1-\varepsilon}{S}. \end{aligned} \quad (42)$$

Notice that the left term is an increasing function of u in the interval $(0, 1)$, which is the interval of interest. In fact, for

$u \rightarrow \{0, 1\}$ the left term converges to $\{0, 1\}$, respectively, and since $\frac{1-\varepsilon}{S} \in (0, 1)$, a unique solution is guaranteed. Now, by relaxing the inequality to an equality and making $g(u) = \frac{1-u}{1-u^S}$, we reformulate (42) as

$$\begin{aligned} u^{S-1} &= \frac{1-\varepsilon}{Sg(u)} \\ u &= \left(\frac{1-\varepsilon}{S}\right)^{\frac{1}{S-1}} g(u)^{-\frac{1}{S-1}}. \end{aligned} \quad (43)$$

Thus, we can say that the unique solution of (43), u^* , is a fixed point of

$$\tilde{g}(u) = \left(\frac{1-\varepsilon}{S}\right)^{\frac{1}{S-1}} g(u)^{-\frac{1}{S-1}}. \quad (44)$$

Now, notice that

$$\begin{aligned} |\tilde{g}(u)'| &= \frac{1}{S-1} \left(\frac{1-\varepsilon}{S}\right)^{\frac{1}{S-1}} g(u)^{-1-\frac{1}{S-1}} |g'(u)| \\ &= \frac{1}{S-1} \left(\frac{1-\varepsilon}{S}\right)^{\frac{1}{S-1}} g(u)^{-1-\frac{1}{S-1}} \left| \frac{S(1-u)u^{S-1} - u(1-u^S)}{(1-u^S)^2} \right| \\ &= \frac{1}{S-1} \left(\frac{1-\varepsilon}{S}\right)^{\frac{1}{S-1}} g(u)^{1-\frac{1}{S-1}} \left| \frac{Su^{S-1} - u(1-u^S)}{1-u} - \frac{u(1-u^S)}{(1-u)^2} \right|, \end{aligned} \quad (45)$$

which reaches the maximum for $\varepsilon = 0$. Fig. 12 shows (45) for such extreme configuration, and since $|\tilde{g}(u)'| < 1$, we can assure that that still holds for any ε . Then, based on the Fixed Point Theory [33] the convergence to the solution is guaranteed by using a fixed point iterative procedure as the one presented in Algorithm 1. Notice that one can choose any $u^{(0)} \in (0, 1)$ as initial value, however, we chose the value shown in line 1 as it already constitutes a good guess towards the final value u^* , which helps to reduce the required number of iterations. Such an initial value comes from realizing that $\frac{1-u^S}{1-u} = \sum_{n=0}^{S-1} u^n > 1 + u^{S-1}$ (using the geometric series) and substituting such result into (42) to attain

$$\begin{aligned} \frac{u^{S-1}}{1+u^{S-1}} &= \frac{1-\varepsilon}{S} \\ u &= \left(\frac{S}{1-\varepsilon} - 1\right)^{-\frac{1}{S-1}}. \end{aligned} \quad (46)$$

For Algorithm 1 to run, we require to specify a tolerance error u_ϵ that we are willing to accept, and it constitutes the stopping criterion. The smaller u_ϵ is, more iterations are required as corroborated in Fig. 12, where it can also be observed that less than 16 iterations are enough in all the cases. Another interesting fact is that the convergence is even faster as S increases. After convergence, L_0 is computed according to line 7, which comes from isolating L in (41).

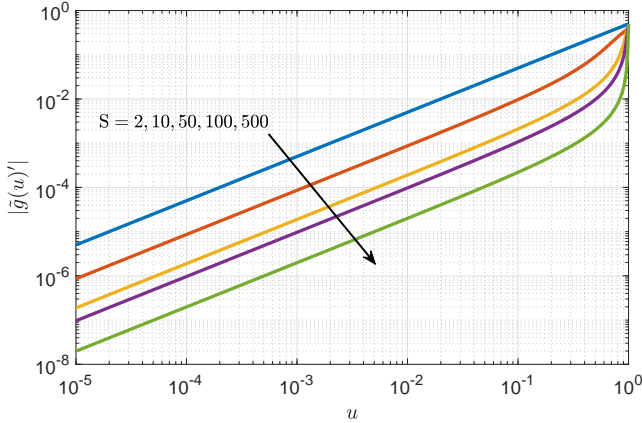
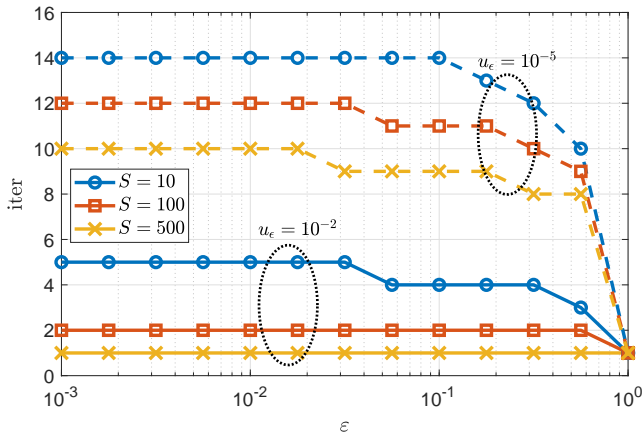
REFERENCES

- [1] M. Latva-aho and K. Leppänen, "Key drivers and research challenges for 6G ubiquitous wireless intelligence," *6G Research Visions*, vol. 1, 2019.
- [2] N. H. Mahmood, S. Böcker, A. Munari, F. Clazzer, I. Moerman, K. Mikhaylov, O. L. A. López, O.-S. Park, E. Mercier, H. Bartz *et al.*, "White paper on critical and massive machine type communication towards 6G," *arXiv preprint arXiv:2004.14146*, 2020.
- [3] "Frost & Sullivan Visionary Innovation Group: Mega Trends." [Online]. Available: <https://ww2.frost.com/research/visionary-innovation/>

Algorithm 1: Finding L_0 (38)**Input :** $S, \varepsilon, t, T_c, \lambda$ and tolerance $u_\varepsilon > 0$ **Output:** L_0, iter

```

1 Initializing:  $u^{(0)} = \left(\frac{S}{1-\varepsilon} - 1\right)^{-\frac{1}{S-1}}$ ,  $\text{iter} = 1, \Delta u = \infty$ 
2 while  $\Delta u > u_\varepsilon$  do
3    $u^{(\text{iter})} := \tilde{g}(u^{(\text{iter}-1)})$  as given in (44);
4    $\Delta u = |u^{(\text{iter})} - u^{(\text{iter}-1)}|$ ;
5    $\text{iter} := \text{iter} + 1$ ;
6 end
7  $L_0 = \left\lceil \frac{t(1-e^{-\lambda})}{(1-u^{(\text{iter})})T_c} \right\rceil$ .
```

Fig. 12. $|\tilde{g}(u)'|$ vs u for $\varepsilon = 0$.Fig. 13. Required number of iterations as a function of ε for Algorithm 1 to converge. We use $S \in \{10, 100, 500\}$ and $u_\varepsilon \in \{10^{-2}, 10^{-5}\}$.

- [4] J. Portilla, G. Mujica, J. Lee, and T. Riesgo, "The extreme edge at the bottom of the Internet of Things: A review," *IEEE Sensors Journal*, vol. 19, no. 9, pp. 3179–3190, May 2019.
- [5] D. Niyato, D. I. Kim, M. Maso, and Z. Han, "Wireless powered communication networks: Research directions and technological approaches," *IEEE Wireless Communications*, vol. 24, no. 6, pp. 88–97, Dec 2017.
- [6] O. L. A. López, H. Alves, R. D. Souza, S. Montejo-Sánchez, E. M. G. Fernández, and M. Latva-aho, "Massive wireless energy transfer: Enabling sustainable IoT towards 6G era," *arXiv preprint arXiv:1912.05322*, 2019.
- [7] A. Ghazanfari, H. Tabassum, and E. Hossain, "Ambient RF energy harvesting in ultra-dense small cell networks: performance and trade-offs," *IEEE Wireless Communications*, vol. 23, no. 2, pp. 38–45, 2016.
- [8] B. Clerckx, R. Zhang, R. Schober, D. W. K. Ng, D. I. Kim, and H. V.

- Poor, "Fundamentals of wireless information and power transfer: From RF energy harvester models to signal and system designs," *IEEE Journal on Selected Areas in Communications*, vol. 37, no. 1, pp. 4–33, Jan 2019.
- [9] N. H. Mahmood, H. Alves, O. L. A. López, M. Shehab, D. P. M. Osorio, and M. Latva-Aho, "Six key features of machine type communication in 6G," in *2nd 6G Wireless Summit (6G SUMMIT)*, 2020, pp. 1–5.
- [10] H. Ju and R. Zhang, "Throughput maximization in wireless powered communication networks," *IEEE Transactions on Wireless Communications*, vol. 13, no. 1, pp. 418–428, January 2014.
- [11] O. L. A. López, H. Alves, R. D. Souza, and E. M. G. Fernández, "Ultra-reliable short-packet communications with wireless energy transfer," *IEEE Signal Processing Letters*, vol. 24, no. 4, pp. 387–391, April 2017.
- [12] W. Huang, H. Chen, Y. Li, and B. Vucetic, "On the performance of multi-antenna wireless-powered communications with energy beamforming," *IEEE Transactions on Vehicular Technology*, vol. 65, no. 3, pp. 1801–1808, March 2016.
- [13] H. Chen, Y. Li, J. L. Rebelatto, B. F. Uchôa-Filho, and B. Vucetic, "Harvest-then-cooperate: Wireless-powered cooperative communications," *IEEE Transactions on Signal Processing*, vol. 63, no. 7, pp. 1700–1711, April 2015.
- [14] O. L. A. López, E. M. G. Fernández, R. D. Souza, and H. Alves, "Wireless powered communications with finite battery and finite blocklength," *IEEE Transactions on Communications*, vol. 66, no. 4, pp. 1803–1816, April 2018.
- [15] O. L. A. López, E. M. G. Fernández, R. D. Souza, and H. Alves, "Ultra-reliable cooperative short-packet communications with wireless energy transfer," *IEEE Sensors Journal*, vol. 18, no. 5, pp. 2161–2177, March 2018.
- [16] B. Makki, T. Svensson, and M. Zorzi, "Wireless energy and information transmission using feedback: Infinite and finite block-length analysis," *IEEE Transactions on Communications*, vol. 64, no. 12, pp. 5304–5318, Dec 2016.
- [17] L. Cantos and Y. H. Kim, "Max-min fair energy beamforming for wireless powered communication with non-linear energy harvesting," *IEEE Access*, vol. 7, pp. 69 516–69 523, 2019.
- [18] R. Du, H. S. Ghadikolaei, and C. Fischione, "Wirelessly-powered sensor networks: Power allocation for channel estimation and energy beamforming," *IEEE Transactions on Wireless Communications*, pp. 1–1, 2020.
- [19] B. Clerckx and J. Kim, "On the beneficial roles of fading and transmit diversity in wireless power transfer with nonlinear energy harvesting," *IEEE Transactions on Wireless Communications*, vol. 17, no. 11, pp. 7731–7743, Nov 2018.
- [20] O. L. A. López, H. Alves, R. D. Souza, and S. Montejo-Sánchez, "Statistical analysis of multiple antenna strategies for wireless energy transfer," *IEEE Transactions on Communications*, vol. 67, no. 10, pp. 7245–7262, Oct 2019.
- [21] O. L. López, S. Montejo-Sánchez, R. D. Souza, H. Alves, and C. B. Papadias, "On CSI-free multi-antenna schemes for massive wireless energy transfer," *arXiv preprint arXiv:2002.03792*, 2020.
- [22] H. Kobayashi, B. L. Mark, and W. Turin, *Probability, random processes, and statistical analysis: applications to communications, signal processing, queueing theory and mathematical finance*. Cambridge University Press, 2011.
- [23] T. A. Khan, R. W. Heath, and P. Popovski, "On wirelessly powered communications with short packets," in *2016 IEEE Globecom Workshops (GC Wkshps)*, Dec 2016, pp. 1–6.
- [24] M. Guillaud, D. T. Stock, and R. Knopp, "A practical method for wireless channel reciprocity exploitation through relative calibration," in *ISSPA*, 2005, pp. 403–406.
- [25] J. Proakis, "Digital communications," 2001.
- [26] N. Nikaein, M. Laner, K. Zhou, P. Svoboda, D. Drajić, M. Popovic, and S. Krco, "Simple traffic modeling framework for machine type communication," in *ISWCS 2013; The Tenth International Symposium on Wireless Communication Systems*, Aug 2013, pp. 1–5.
- [27] A. Thudugalage, S. Atapattu, and J. Evans, "Beamformer design for wireless energy transfer with fairness," in *2016 IEEE International Conference on Communications (ICC)*, 2016, pp. 1–6.
- [28] Y. Ye, *Interior point algorithms: theory and analysis*. John Wiley & Sons, 2011, vol. 44.
- [29] D. Hernandez-Stumpfhauser, F. J. Breidt, M. J. van der Woerd *et al.*, "The general projected normal distribution of arbitrary dimension: modeling and Bayesian inference," *Bayesian Analysis*, vol. 12, no. 1, pp. 113–133, 2017.
- [30] C. Siriteanu, Y. Miyanaga, S. D. Blostein, S. Kuriki, and X. Shi, "MIMO Zero-Forcing detection analysis for correlated and estimated Rician

- fading,” *IEEE Transactions on Vehicular Technology*, vol. 61, no. 7, pp. 3087–3099, Sep. 2012.
- [31] H. Gao, P. J. Smith, and M. V. Clark, “Theoretical reliability of MMSE linear diversity combining in Rayleigh-fading additive interference channels,” *IEEE Transactions on Communications*, vol. 46, no. 5, pp. 666–672, May 1998.
- [32] H. Lim and D. Yoon, “On the distribution of SINR for MMSE MIMO systems,” *IEEE Transactions on Communications*, vol. 67, no. 6, pp. 4035–4046, June 2019.
- [33] R. Agarwal, M. Meehan, and D. O’regan, *Fixed point theory and applications*. Cambridge university press, 2001, vol. 141.